Communication between the Nucleotide Binding Domains of P-Glycoprotein Occurs via Conformational Changes that Involve Residue 508[†]

Mark P. Gabriel,[#] Janet Storm,[#] Alice Rothnie,[#] Andrew M. Taylor,[#] Kenneth J. Linton,[‡] Ian D. Kerr,[#,§] and Richard Callaghan*[,#]

Nuffield Department of Clinical Laboratory Sciences, John Radcliffe Hospital, University of Oxford, OX3 9DU, UK, MRC Clinical Sciences Centre, Imperial College School of Medicine, Hammersmith Hospital, London, W12 0NN, UK, and School of Biomedical Sciences, University of Nottingham, Queen's Medical Centre, Nottingham, NG7 2UH, UK

Received January 20, 2003; Revised Manuscript Received April 30, 2003

ABSTRACT: Our aim is to provide molecular understanding of the mechanisms underlying the (i) interaction between the two nucleotide binding domains (NBDs) and (ii) coupling between NBDs and transmembrane domains within P-glycoprotein (Pgp) during a transport cycle. To facilitate this, we have introduced a number of unique cysteine residues at surface exposed positions (E393C, S452C, I500C, N508C, and K578C) in the N-terminal NBD of Pgp, which had previously been engineered to remove endogenous cysteines. Positions of the mutations were designed using a model based on crystallographic features of prokaryotic NBDs. The single cysteine mutants were expressed in insect cells using recombinant baculovirus and the proteins purified by metal affinity chromatography by virtue of a polyhistidine tag. None of the introduced cysteine residues perturbed the function of Pgp as judged by the characteristics of drug stimulated ATP hydrolysis. The role of residues at each of the introduced sites in the catalytic cycle of Pgp was investigated by the effect of covalent conjugation with *N*-ethyl-maleimide (NEM). All but one mutation (K578C) was accessible to labeling with [^{3}H]-NEM. However, perturbation of ATPase activity was only observed for the derivitized N508C isoform. The principle functional manifestation was a marked inhibition of the "basal" rate of ATP hydrolysis. Neither the extent nor potency to which a range of drugs could affect the ATPase activity were altered in the NEM conjugated N508C isoform. The results imply that the accessibility of residue 508, located in the α-helical subdomain of NBD1 in Pgp, is altered by the conformational changes that occur during ATP hydrolysis.

Overexpression of the multidrug transporter P-glycoprotein (Pgp)[1] is one of the major mechanisms leading to multidrug resistance in cancer (*1*, *2*). Pgp (ABCB1) is a member of the ATP-Binding Cassette (ABC) transporter family, and comprises two cytoplasmic nucleotide-binding domains (NBDs) and two transmembrane domains (TMDs) (*3*). ATP is hydrolyzed at the NBDs to provide energy for the transport of the drugs that interact with Pgp in the TMDs (*4*−*8*). The expression and function of Pgp confer resistance to many structurally and functionally unrelated cytotoxic drugs in various forms of cancer (*2*). Several studies have demonstrated that within the TMDs there are a number of distinct binding sites, with specificity for different classes of drugs (*6*, *9*, *10*). Furthermore, an allosteric communication network between the different drug binding sites has been demonstrated (*9*) to underlie the complex profile of pharmacological interactions observed for Pgp (*11*). The binding of drugs to these sites in the TMDs is coupled to the hydrolysis of ATP in the NBDs, as shown by (i) the increased rate of ATP hydrolysis in the presence of drugs (ii) the effects of ATP binding on drug affinity constants and (iii) structural changes in the TMDs induced by nucleotide interaction (*12*−*14*). Both NBDs can bind and hydrolyze ATP (*15*); however, total inhibition of ATP hydrolysis by Pgp is observed by perturbation of a single NBD (*16*−*18*). This experimental evidence has led to the alternating sites model for ATP hydrolysis by Pgp (*19*), which is dependent on efficient coupling between these two catalytic domains.

The coupling between the two NBDs and between the TMDs and NBDs is thought to occur by conformational changes in the protein at discrete stages of the catalytic cycle. Numerous technical approaches such as differential trypsin digest patterns (*20*), changes in accessibility of the extracellular UIC2 epitope (*21*) and fluorescence quenching, both intrinsic (*22*) and for covalently attached probes (*23*) have demonstrated such intraprotein conformational changes.

[†] This work was supported by a Cancer Research UK program grant, a BBSRC studentship (M.G.), an MRC Studentship (A.R.), and a Wellcome Trust Fellowship for I. D. Kerr.

* To whom all correspondence should be addressed. E-mail richard.callaghan@ndcls.ox.ac.uk. Fax: +44 1865 221 834. Telephone: +44 1865 221 110.

[#] University of Oxford.

[‡] Imperial College School of Medicine.

[§] University of Nottingham.

[1] Abbreviations: Pgp, P-glycoprotein; NBD, nucleotide binding domain; ABC, ATP binding cassette; NEM, *N*-ethyl-maleimide; TMDs, transmembrane domains; ICDs, intracellular domains; BtuCD, *E. coli* vitamin B_{12} transporter; MsbA, *E. coli* lipid A transporter; Rad50, ATP binding/catalytic domain involved in prokaryotic DNA double strand break repair; AMP−PNP, 5′-adenylyl imidophosphate; CFTR, cystic fibrosis transmembrane conductance regulator; HisP, histidine permease nucleotide binding domain; MalK, maltose transporter nucleotide binding domain; DMSO, dimethyl sulfoxide; MOPS, 3-(*N*-morpholino)-propanesulfonic acid; ANOVA, one way analysis of variance.

10.1021/bi0341049 CCC: $25.00
Published on Web 06/06/2003

Furthermore, electron microscopy has also shown distinct structural alterations for Pgp during ATP binding and subsequent hydrolysis (*13*, *24*). Unfortunately, there is no information regarding the regions/residues involved, or the molecular mechanisms underlying the conformational changes.

High-resolution structures of the NBDs from a number of ABC transporters have been determined by crystallography (*25*−*27*), but have only served to stimulate further controversy surrounding NBD−NBD interactions. The reported structures of these monomers all share a similar protein fold with three subdomains: an F_1-like ATPase subdomain, a β-sheet subdomain, and one comprising high α-helical content. The three subdomains are arranged such that the NBD adopts an overall "L"-shape. Controversy surrounding the exact orientation of the two NBDs in the intact transporter (*28*) has been reawakened by recent structures of prokaryotic ABC transporters (MsbA and BtuCD) with NBDs and cognate TMDs, which offer alternative depictions of the assembled transporter (*29*, *30*). The structure of the bacterial lipid A transporter, MsbA, suggests little direct interaction between the NBDs, but describes a direct interaction between the NBD and its cognate TMD via an intracellular domain (ICD). However, the structural data for MsbA suffers from unresolved density within the NBDs. In contrast, the BtuCD structure does not contain ICDs and suggests a lack of interaction between the N-terminal NBD with the C-terminal TMD, and vice versa. Moreover, the TMDs of BtuCD do not have the same number of transmembrane α-helices or architecture as the MsbA structure. Thus, the TMDs of the BtuCD and MsbA transporters are nonhomologous, and therefore communication between their respective NBDs and TMDs is likely to be different. It remains unclear which residues or regions of ABC proteins are involved in the transmission of conformational changes during a transport cycle.

Our investigations have begun to address the nature of the domain/domain interfaces utilizing the cysteine-scanning mutagenesis approach. It is reasonable to assume that interdomain interactions are likely to occur at the interface between the two NBDs and between the NBDs and TMDs. Using a molecular model of the N-terminal NBD of Pgp, based on the available prokaryotic structures, cysteine residues were introduced at a number of surface exposed regions. The effect of these mutations on the function of Pgp were characterized and any changes in ATPase activity after derivitization with the thiol specific probe NEM were investigated. Finally, alterations in the accessibility of these regions to the thiol specific probe at different stages of the transport cycle were investigated. These results identified residue 508 as undergoing changes in solvent accessibility during catalytic cycle conformational changes. Analysis of the data was consistent with an orientation of NBDs in Pgp that is similar to that in Rad50, MJ0796, and BtuCD (*26*, *29*, *33*).

EXPERIMENTAL PROCEDURES

Materials. Escherichia coli lipids were purchased from Avanti Polar Lipids (Alabaster, USA). Octyl-β-D-glucoside, AMP−PNP, and SM2-Biobeads were obtained form CN Biosciences (Nottingham, UK). All restriction enzymes were purchased from New England Biolabs (Hitchin, UK), the vector pBakPAK9 from Clontech (Basingstoke, UK) and the Altered Sites II mutagenesis kit from Promega (Southampton, UK). The anti-Pgp (C219), and anti-$(His)_n$ monoclonal antibodies were purchased from CIS (Gif-Sur-Yvette, France) and Invitrogen (Groningen, The Netherlands), respectively. [^{3}H] Phosphatidyl choline (83 Ci/mmol), [^{3}H] *N*-ethyl-maleimide (52 Ci/mmol), and [α-^{32}P]-8-azido-ATP (2−10 Ci/mmol) were obtained from Amersham-Pharmacia (Amersham, UK), NEN Pharmaceuticals (Hounslow, UK) and ICN Chemicals (Basingstoke, UK), respectively. XR9576 was provided as a generous a gift from Xenova Ltd (Slough, UK), while disodium adenosine triphosphate (Na_2ATP), cholesterol, sodium orthovanadate, nicardipine, vinblastine sulfate, paclitaxel, bovine serum albumin (99% purity), and *N*-ethyl-maleimide (NEM) were purchased from Sigma Chemicals (Poole, UK). All other general chemicals were of at least analytical grade.

Table 1: Oligonucleotide Sequences Employed to Introduce Single Cysteine Mutations into Pgp[a]

mutation	restriction site	sequence (5′-3′)
E393C	−EcoRI	GA AAT TTG tgt TTC AGA AAT
R395C	−EcoRI	TTG GAg TTC tGt AAT GTT CAC
M450C	+HinCII	GAG GGG tgt GTC AGT GTT GAc GGA CAG
S452C	+HinCII	GGG ATG GTC tGT GTT GAc GGA CAG

[a] Lowercase is used to denote mutated bases, while underlined triplets denote introduced codons for cysteine. Mutations outside of the introduced cysteine codons are silent with respect to protein sequence and facilitate the tracking of mutagenesis and DNA subcloning by altering the restriction digest profile as indicated.

Molecular Model of the N-Terminal NBD of Pgp. The amino acid sequence of Pgp NBD1 was aligned with a number of other NBDs including Pgp NBD2, both NBDs of CFTR and several well-characterized NBDs of bacterial transport systems, including HisP and MalK. From this, a pairwise alignment of Pgp NBD1 and HisP was extracted and visually inspected to ensure that secondary structural elements present within the HisP crystal structure were not interrupted by insertions or deletions in the alignment. An initial homology model for Pgp NBD1 was then generated by the program Modeler (*31*) employing HisP as a structural template (*25*). HisP was chosen over other solved crystal structures (such as MalK (*27*) or MJ0796 (*32*, *33*)) because it is a well-characterized protein biochemically, and the structure is resolved to a high resolution (1.5 Å). Furthermore, HisP is crystallized in the presence of ATP, which is found coordinated by the conserved Walker motifs of the NBD (*25*). The initial model of Pgp was refined within Modeler, employing restraints to maintain the conserved secondary structural regions of NBD proteins (*28*). Iterations of the modeling process produced a family of molecular models for Pgp NBD1.

Generation of Mutant Pgp Isoforms. Of the 10 desired mutations (see Results), six had been previously made by us as constructs suitable for transient mammalian transfection (*34*). These mutations were introduced into the plasmid pBacPAK9_MDR-cys$^-$ by subcloning. The remaining four single cysteine mutations were introduced into the coding sequence of cysteine-less Pgp using the oligonucleotide primers given in Table 1. In each case, the primer introduced the desired cysteine residue (underlined) and also a silent,

diagnostic restriction enzyme site to facilitate identification of mutated plasmids. Following successful mutation, the mutants were introduced into pBacPAK9_ MDR-cys$^-$ by DNA subcloning. Fidelity of mutations was confirmed by nucleotide sequencing (Department of Biochemistry, University of Oxford). Plasmids generated in this manner are referred to by the nomenclature pBP9C−XnC, representing pBacPAK9-MDR-Cys$^-$ encoding a mutation from residue type *X* at position *n* to a unique cysteine (*C*).

Generation of Recombinant Baculovirus for Mutant Isoforms of Pgp. Insect cell lines *Spodoptera frugiperda* (Sf9) and *Trichoplusia ni* (High Five) were maintained in serum free medium (SF-900II; Life Technologies, UK), or Ex-cell 405 medium; (JRH Biosciences, USA), respectively, as previously described (*35*). Recombinant baculovirus was obtained by lipofectin-mediated cotransfection of pBP9C−XnC plasmids and BacPAK6-viral DNA. Recombinant virus was purified and amplified by two consecutive rounds of plaque assay, performed according to standard procedures (*36*).

Expression, Purification, and Reconstitution of Mutant Pgp Isoforms in Insect Cells. We have previously described in detail the expression of Pgp isoforms in insect cells and their subsequent purification and reconstitution (*35*). Briefly, mutant isoforms of Pgp were expressed in High Five cell suspensions (1.5×10^6 cells/mL) by infection with recombinant virus at a multiplicity of infection of five. Cells were harvested 3 days later by centrifugation (2000*g*, 10 min, 4 °C). Cell membranes were isolated by nitrogen cavitation and stored in buffer comprising 0.25 M sucrose, 10 mM Tris pH 7.4 at −80 °C for up to 8 months. The Pgp containing membranes were pelleted by centrifugation at (100000*g*, 4 °C, 20 min) and solubilized with 2% (w/v) octyl-β-D-glucoside in buffer 1 (20 mM Tris pH 6.8, 150 mM NaCl, 1.5 mM $MgCl_2$, 20% (v/v) glycerol, 1 mM benzamidine, 1 μM pepstatin A, 20 μM leupeptin). This buffer was also supplemented with 0.4% (w/v) of a 4:1 (w/w) mixture of *Escherichia coli* total lipid extract and cholesterol. Pgp was purified using immobilized metal affinity chromatography (nickel-NTA Superflow) and eluted from the resin in buffer 1 supplemented with 1.25% (w/v) octyl glucoside, 0.1% (w/v) lipid mixture, and 120 mM imidazole. Reconstitution was achieved by removal of detergent from Pgp containing fractions with adsorbent SM2-BioBeads, which resulted in lipid/protein ratios of approximately 50 (w/w), or 8800 (mol/mol). Reconstitution efficiency was demonstrated by comigration of Pgp and lipids in sucrose gradient density centrifugation as previously described (*35*).

ATPase Activity of Purified Mutant Pgp Isoforms. The ATPase activity of purified reconstituted Pgp was determined by measuring the liberation of inorganic phosphate using a modified colorimetric assay (*37*). The buffer consisted of 50 mM Tris (pH 7.4), 150 mM NH_4Cl, 5 mM $MgSO_4$, 0.02% (w/v) NaN_3. Purified, reconstituted protein (∼250 ng) was incubated at 37 °C for 20 min, during which time the activity is linear (*35*). To determine Michealis−Menten parameters (K_m, V_{max}) the protein was incubated at varying ATP concentrations (0−2 mM) either in the absence (basal) or presence (drug stimulated) of a fixed nicardipine concentration (30 μM). The potency of drugs to stimulate, or inhibit, the ATPase activity was determined using a range of concentrations of drug (3 nM to 100 μM) at a fixed concentration of ATP (2 mM). The inhibition studies were prestimulated with 30 μM nicardipine. The effect on the ATPase of labeling the cysteine-modified Pgp mutants was tested by preincubation of protein (∼250 ng) for 30 min with *N*-ethyl-maleimide (NEM) at 20 °C prior to addition of ATP as described above.

[^{3}H]-NEM Labeling of Mutant Pgp Isoforms. The radioisotope [^{3}H]-NEM was utilized as a cysteine modifying compound due to its specific covalent derivitization of free suphydryl groups in the pH range 6.5−7.5. To determine the relative propensities of the various Pgp mutant isoforms to undergo such derivitization, purified protein (250 ng) was incubated with 0.01−1 μM [^{3}H]-NEM for 1 h at 20 °C in a total volume of 40−50 μL. The [^{3}H]-NEM was added from a concentrated stock in DMSO to ensure that the final solvent concentration was ≤2% (v/v). Control investigations had determined that the presence of DMSO up to 5% (v/v) had no effect on labeling. These conditions resulted in a probe/protein ratio in excess of 50 to ensure high labeling efficiency and prevent excessive depletion of the radioligand following the irreversible reaction with accessible cysteine residues. Furthermore, previous data have shown that at this high molar excess, reactivity remains specific to cysteine at pH 6.8. Following the appropriate incubation period, the reaction was terminated by the addition of Laemmli sample buffer containing 5% (v/v) β-mercaptoethanol to quench unreacted [^{3}H]-NEM. Unbound [^{3}H]-NEM was separated from labeled Pgp mutants by SDS−PAGE (7.5% acrylamide), and protein was then fixed in 25% (v/v) 2-propanol, 10% (v/v) acetic acid for 30 min. The gels containing fixed [^{3}H]-NEM labeled protein were placed in Amplify (Amersham) for 30 min to enable detection of the radiolabel by autoradiography. Images were scanned and transferred to Scion Image Software (www.scioncorp.com) to quantify density of the bands. A number of exposures were employed for each gel to ensure that signals were within the linear range.

The time course of [^{3}H]-NEM association with the N508C Pgp was determined by incubating protein (250 ng) for 1−240 min (20 °C) with [^{3}H]-NEM (1 μM). Following incubation, the reaction was terminated as described above. To determine the effect of nucleotide on accessibility of N508C Pgp to covalent modification the protein (250 ng) was incubated with the non-hydrolysable ATP analogue AMP−PNP (0−10 mM) in buffer comprising 100 mM MOPS pH 6.8 and 5 mM $MgCl_2$. This buffer was chosen to prevent significant pH drop at high nucleotide concentrations. Following 30-min incubation at 20 °C, [^{3}H]-NEM (1 μM) was added for a further period of 60 min and samples treated as above to determine the extent of labeling.

Labeling efficiency of the N508C Pgp trapped in a posthydrolytic conformation was tested following a vanadate trapping procedure based on previously published methods (*12*). Vanadate (200 μM) and ATP (2 mM) were added to the protein and incubated at 37 °C for 30 min to ensure full inhibition and generation of the catalytic intermediate. [^{3}H]-NEM (0.1−3 μM) was then added to samples (1 h, 20 °C) and the extent of labeling was determined as described above.

[^{32}P]-Azido-ATP Photoaffinity Labeling of Pgp. The photoaffinity labeling of wild type and N508C Pgp was based on previously published methods (*12*−*14*). Protein (250 ng) was incubated with [α-^{32}P]-azido-ATP (3 μM) at 20 °C for 20 min in the dark in a reaction volume of 70 μL to reach

binding equilibrium. Buffer comprised 100 mM MOPS pH 6.8 and 20% (v/v) glycerol, the latter added to scavenge nonspecific, photoinduced free radical species. Samples were then placed in ice and subjected to UV-irradiation (100 W at 5 cm) for 5 min and the products were separated from unreacted [^{32}P]-azido-ATP by SDS−PAGE. The photolabeled Pgp was then detected by autoradiography at −80 °C and the radiosignal quantified using densitometry as described above. To assess the effect of NEM, the wild type or N508C isoforms were incubated with 100 μM NEM, in the dark for 1 h prior to the addition of [α-^{32}P]-azido-ATP.

Data Analysis. The Michaelis−Menten parameters of maximal velocity (V_{max}) and ATP affinity (K_m) were obtained from nonlinear regression of the following equation:

$$v = (V_{max}[S])/(K_m + [S]) \quad (1)$$

where v = enzyme activity (μmol of Pi min^{-1} mg^{-1}); V_{max} = maximal ATPase activity (μmol of Pi min^{-1} mg^{-1}); K_m = affinity for ATP (mM); [S] = substrate concentration (mM).

The potency and extent of drugs to alter ATPase activity were obtained by nonlinear regression of the general dose−response equation:

$$V = V_{min} + (V_{max} - V_{min})/(1 + 10^{(\log EC50 - L)}) \quad (2)$$

where V = fraction maximal response; V_{min} = minimal response; V_{max} = maximal response; EC_{50} = ligand concentration producing 50% of maximal response; L = logarithm of drug concentration.

The time-course for [^{3}H]-NEM labeling of the N508C mutant Pgp isoform was fitted by a single phase association equation:

$$B = B_{max}(1 - \exp^{-kt}) \quad (3)$$

where B = fraction bound; B_{max} = maximal binding; k = association rate constant (min^{-1}); t = time (min).

The rate constant was converted to the half-life for association by the relationship $t_{1/2} = 0.69/k$.

Statistical comparisons of two sample means were achieved by an unpaired Student's *t*-test, while multiple comparisons were performed using ANOVA with a Tukey's post-hoc test. In all cases, a $P < 0.05$ was considered statistically significant. All nonlinear regression was done using GraphPad Prism 3.0.

RESULTS

NBD1 Residues Potentially Located at a Domain Interface. Residues on the surface of Pgp NBD1 will potentially be located at the NBD/NBD or NBD/TMD interfaces in the intact transporter. To assist in identification of candidate residues we have employed a homology modeling strategy involving (i) selection of a template structure (HisP) (*25*), (ii) alignment of the template with the target, and (iii) generation of a family of molecular models. One such model is shown in a ribbon representation in Figure 1. The model presented was selected as the basis for our identification of candidate residues based upon having acceptable stereochemistry (as determined by the structural analysis program Procheck) (*38*). Additional visual inspection was employed

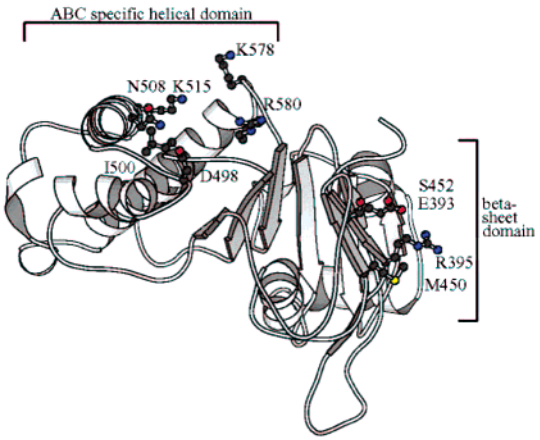

FIGURE 1: Model of the N-terminal nucleotide binding subdomain of Pgp. The model depicts the α-carbon "backbone" of Pgp NBD1. Residues selected for mutation are shown in red with side-chains in ball-and-stick format. Numbers indicate the positions of the residues in Pgp.

to confirm that the orientation of ATP-coordinating residues (*28*) was similar to that observed in the crystal structure template (*25*). As expected, our model adopts the characteristic L-shape domain structure as displayed by numerous NBDs (*25*, *27*, *39*).

The 10 residues identified for mutagenesis are displayed in ball-and-stick format in Figure 1. The criterion for residue selection was that the side-chains of the amino acids should be exposed on the surfaces of the model. Residues were only considered if they were either on the upper surface of the ABC α-helical subdomain (top surface in Figure 1), or on the surface of the β-sheet ABC-specific subdomain (right-hand face in Figure 1). Residues exposed on the "inside" of the L-shape domain were not considered for mutation since these may cause undesirable effects on the structure of the ATP binding pocket (*25*, *28*).

Expression and Purification of Pgp Mutants. The amino acids identified above were mutated individually to cysteine in human Pgp in which the seven native cysteine residues had been replaced by serine, and in which a C-terminal hexahistidine tag had been engineered to facilitate purification (*35*). This parent protein is termed Cys-less, and single-cysteine isoforms derived from this are referred to as, for example, N508C, denoting that the asparagine at position 508 has been mutated to cysteine. We were able to demonstrate Pgp expression for five of the 10 mutant isoforms desired. Although recombinant virus was produced for R395C, M450C, D498C, and K515C (determined by hybridization of radiolabeled anti-*mdr1* oligonucleotides to DNA isolated from recombinant virus), we were unable to detect Pgp expression following insect cell infection. No recombinant virus could be obtained for R580C despite several independent cotransfection experiments. Therefore, our investigations concentrated on three mutations located on the α-helical subdomain (I500C, N508C, K578C) and two on the surface of the β-sheet ABC-specific subdomain (E393C, S452C).

A typical membrane preparation (100 mg of protein) produced a yield of 159 ± 36 μg of purified wild type Pgp, suggesting that the protein accounts for approximately 0.2% of total membrane protein. Similar yields were obtained for Cys-less (105 ± 23 μg), N508C (121 ± 28 μg), K578C

Table 2: The Effects of Cysteine Replacement on Characteristics of ATP Hydrolysis[a]

		basal ATPase activity		stimulated ATPase activity		fold
Pgp isoform	*n*	K_m (mM)	V_{max} (μmol/min/mg)	K_m (mM)	V_{max} (μmol/min/mg)	stimulation
Cys-less	10	0.52 ± 0.05	0.29 ± 0.06	0.37 ± 0.04	0.83 ± 0.12	2.9 ± 0.2
E393C	3	0.39 ± 0.03	0.47 ± 0.25	0.18 ± 0.01	1.41 ± 0.48	3.4 ± 0.8
S452C	4	0.39 ± 0.03	0.49 ± 0.13	0.31 ± 0.04	1.19 ± 0.37	2.4 ± 0.7
I500C	4	0.20 ± 0.03	0.24 ± 0.07	0.24 ± 0.04	0.51 ± 0.21	2.6 ± 0.2
N508C	4	0.54 ± 0.12	0.21 ± 0.09	0.38 ± 0.03	0.52 ± 0.10	3.2 ± 0.5
K578C	4	0.64 ± 0.17	0.31 ± 0.13	0.35 ± 0.05	0.54 ± 0.21	2.0 ± 0.2

[a] ATPase activity was measured for each mutant isoform of Pgp as described in Materials and Methods. Basal activity is that measured in the absence of drug while stimulated activity was determined in the presence of 30 μM nicardipine. Protein (250 ng) was incubated with varying concentrations of Mg·ATP (0−2 mM) for a period of 20 min at 37 °C. Data were fitted by the Michaelis−Menten equation using nonlinear regression and values shown represent mean ± SEM of multiple independent protein preparations. K_m refers to the affinity for ATP, while V_{max} corresponds the maximal rate of hydrolysis. *n* refers to the number of independent observations. Fold-stimulation refers the degree to which nicardipine increased the basal V_{max}.

(118 ± 29 μg), while the amount of I500C (54 ± 22 μg) was approximately half. Unfortunately, mutants E393C (5 ± 0.4 μg) and S452C (13 ± 3 μg) produced significantly lower yields despite several attempts to increase expression by producing higher titer recombinant baculovirus. The reconstitution of all mutant isoforms was similar to wild type, the efficiency of which has been previously described (*35*).

Assessment of the Function of the Mutant Pgp Isoforms. The characteristics of ATP hydrolysis were determined for each cysteine-containing mutant and compared to the Cys-less protein. The latter was chosen as the control, or reference, protein due to its previously reported similarity in functional characteristics to wild-type Pgp (*35*). Maximal rates of ATP hydrolysis (V_{max}) and ATP affinity (K_m) were obtained under basal and drug stimulated (30 μM nicardipine) conditions and the results shown in Table 2. In the absence of drug, the various isoforms of Pgp displayed maximal rates of ATP hydrolysis in the range 0.21−0.49 μmol min^{-1} mg^{-1}, and there were no significant differences compared to Cys-less as determined by ANOVA. The ATPase activity of each cysteine mutant Pgp was stimulated by nicardipine (range = 0.51−1.4 μmol min^{-1} mg^{-1}). The values for K_m were in the range 0.2−0.5 mM and none of the values obtained for mutant proteins was significantly different to the Cys-less protein (ANOVA). Furthermore, the degree to which nicardipine stimulated ATP hydrolysis was similar in all mutant isoforms. These results indicate the basic characteristics of ATP hydrolysis (K_m, V_{max}) were preserved following introduction of cysteine residues and that for nicardipine, the allosterically mediated stimulation in ATP hydrolysis was largely unaffected.

However, Pgp contains several distinct drug-binding sites within the transmembrane domains, and it is possible that independent routes of communication to the NBDs exist. Consequently, the ability of nicardipine, the transported substrate vinblastine, the potent allosteric modulator XR9576 and the metabolic inhibitor vanadate to affect ATP hydrolysis were determined. Complete dose−response analyses (3 nM to 100 μM) were obtained for each drug using saturating concentrations of ATP (2 mM) and the potency to elicit a response (EC_{50} or IC_{50}) determined by nonlinear regression (Table 3). Nicardipine and vinblastine produced dose-dependent increases in ATP hydrolysis with similar potency. Moreover, the potency for stimulation did not significantly differ from Cys-less for any mutant (ANOVA). XR9576 was able to affect ATP hydrolysis in each mutant with greater potency than vinblastine or nicardipine; however, the nature of the effect was inhibitory. The degree of inhibition varied from 78 ± 3% for S452C to 87 ± 1% for N508C and the IC_{50} values were in the range 0.55−0.8 μM. Similarly to the stimulatory drugs, the potency for XR9576 to affect ATP hydrolysis was not different in any mutant compared to Cys-less. The final compound examined was vanadate (Vi), which produces the stable catalytic intermediate complex Mg·ADP·Vi-Pgp. Vanadate produced between 91 ± 3% (N508C) and 99 ± 1% (Cys-less) inhibition of overall ATPase activity. The inhibitory potencies produced by vanadate were less than observed for XR9576; however, there were no statistically significant differences between the mutants (ANOVA).

Table 3: The Effects of Cysteine Replacement on Drug Stimulation or Inhibition of ATP Hydrolysis[a]

	nicardipine	vinblastine	XR9576	vanadate
Pgp isoform	EC_{50} (μM)	EC_{50} (μM)	IC_{50} (μM)	IC_{50} (μM)
Cys-less	6.3 ± 0.1	4.6 ± 1.3	0.79 ± 0.27	3.4 ± 1.3
E393C	4.4 ± 1.4	10.8 ± 4.2	0.79 ± 0.16	4.6 ± 1.1
S452C	2.9 ± 0.8	8.2 ± 3.4	0.61 ± 0.24	4.9 ± 0.4
I500C	3.0 ± 0.6	5.4 ± 0.7	0.80 ± 0.19	5.1 ± 0.9
N508C	5.8 ± 0.9	6.2 ± 2.9	0.55 ± 0.15	7.4 ± 1.8
K578C	7.7 ± 0.5	12.4 ± 2.1	0.57 ± 0.11	4.3 ± 0.8

[a] ATPase activity was measured for each Pgp isoform in the presence of 2 mM Mg·ATP with varying concentrations (3 nM to 100 μM) of either stimulatory drugs (nicardipine, vinblastine) or inhibitors (XR9576, vanadate). The two inhibitors were added in conjunction with 30 μM nicardipine to assess their effects on stimulated ATPase activity. The potency (EC_{50}) to which each compound was able to affect ATPase activity was derived from nonlinear regression of the general dose−response equation. All values represent the mean ± SEM obtained from at least three independent protein preparations.

ATP hydolysis and its stimulation by drugs is a critical process in Pgp mediated transport and thus provides a sensitive measure of protein function. The results presented above indicate that replacement of the indicated endogenous residues in the N-terminal NBD by cysteine did not perturb the catalytic cycle or drug induced communication between the transmembrane and nucleotide binding domains.

The Effects of the Cysteine Reactive Compound NEM on ATPase Activity of Mutant Pgp Isoforms. Although mutation of residues E393, S452, I500, N508, or K578 to cysteine did not significantly change the ATPase activity of Pgp and suggests that none of the residues is directly involved in the catalytic process. It is possible that for some of these residues, substitution by cysteine may be sufficiently conservative to maintain function and mask a role in communication. To

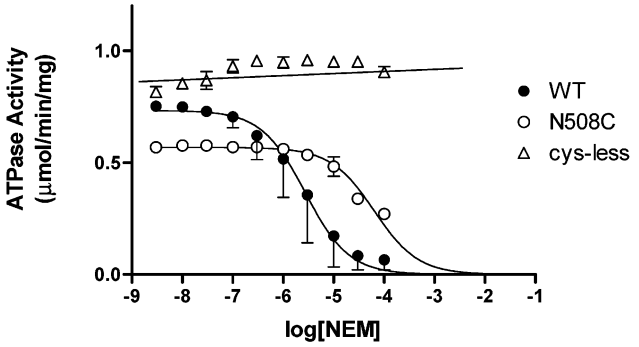

FIGURE 2: The effects of [^{3}H]-NEM labeling on the ATPase activity of wild-type Pgp, cysteine-less Pgp (Cys-less) and the N508C mutant. ATPase activity (μmol/min/mg) of purified Pgp (250 ng) was measured as described in experimental procedures using 2 mM Mg·ATP, 30 μM nicardipine and a range of NEM concentrations (3 nM to 100 μM). The effect of NEM on this activity was fitted by the general dose−response relationship and the data represents the mean ± SEM from 3 to 5 determinations.

address this possibility, the individual residues were covalently modified with the sulfydryl specific compound NEM. Following derivitization with varying concentrations of NEM the maximal rate of ATP hydrolysis (i.e., at 2mM ATP) was measured for each mutant protein. Figure 2 shows data depicting the effects of covalent modification on drug stimulated ATPase activity in wild type, Cys-less and N508C Pgp. Activity of wild type Pgp was completely inhibited by NEM (IC_{50} = 6.5 ± 0.5 μM), which is consistent with the presence of seven cysteine residues in various locations, including one adjacent to the critical lysine residue of each Walker A motif. The specificity of labeling to cysteine residues was confirmed by the lack of effect (2.7 ± 1.2% inhibition) on the Cys-less mutant Pgp isoform.

None of the mutants E393C (2.3 ± 2.1%), S452C (2.2 ± 1.9%), I500C (1.9 ± 1.2%), nor K578C (3.1 ± 1.1%) displayed significant inhibition of the drug stimulated ATPase activity in the presence of up to 100 μM NEM (data not shown). In contrast, NEM was able to inhibit the ATPase activity of N508C characterized by a potency of IC_{50} = 15 ± 3 μM. These results suggest that either (i) only mutant N508C isoform is accessible to labeling with NEM or (ii) only residue 508C is involved in the catalytic process in Pgp.

Characterization of Pgp Labeling by [^{3}H]-NEM. To ascertain which of the two possibilities had occurred, each mutant isoform was incubated with [^{3}H]-NEM to determine whether the introduced cysteine residue was accessible to derivitization. Figure 3a demonstrates representative autoradiograms of the relative labeling of wild-type Pgp and the mutant N508C isoform with varying concentrations of radiolabel (0.01−1 μM). The mutant proteins (250 ng) were incubated with 1 μM radiolabel, which represents a 50-fold molar excess. Wild type Pgp displayed the highest degree of labeling, which is consistent with the presence of multiple cysteine residues. The maximal extent of labeling observed for the wild type Pgp was arbitrarily assigned a value of 1.0 to facilitate comparisons between the various mutants (Table 4). Negligible labeling was observed for the Cys-less and the K578C mutant Pgp isoforms. The inability to label mutant K578C correlates with the lack of effect of NEM on the ATPase activity of this mutant Pgp isoform. Specificity of NEM for cysteine residues was confirmed by the absence of any labeling on the Cys-less protein. The E393C and

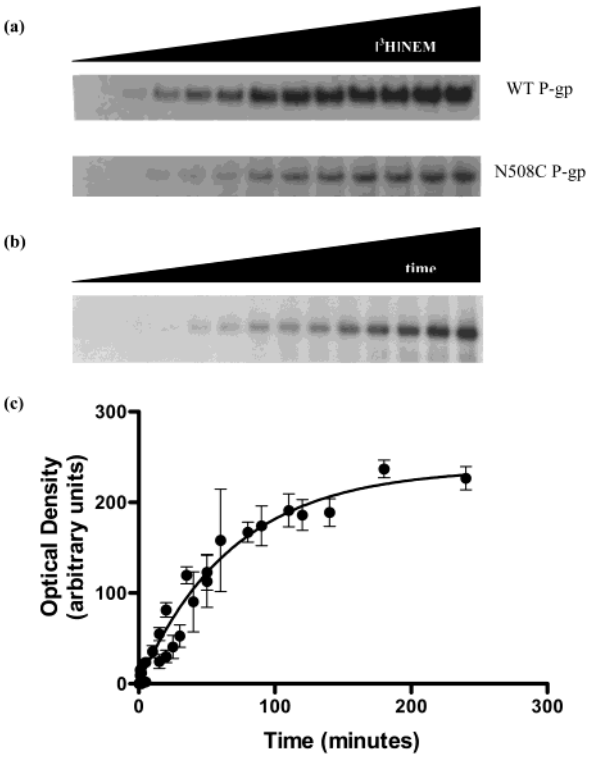

FIGURE 3: Labeling of Pgp with [^{3}H]-NEM. (a) A representative autoradiogram showing the relative labeling of purified wild type and N508C Pgp. Protein (250 ng) was incubated with varying concentrations of [^{3}H]-NEM (0.01−1 μM) for 1 h at 20 °C. The reaction was quenched by β-mercaptoethanol and proteins separated by SDS−PAGE. Binding of [^{3}H]-NEM was observed by autoradiography. (b) Purified, reconstituted N508C (250 ng) was incubated with 1 μM [^{3}H]-NEM for indicated times at 20 °C. (c) Quantitation of the Pgp associated band intensity was performed as described in the text and the mean graph obtained from four such experiments is plotted.

Table 4: The Ability of [^{3}H]-NEM to Label Pgp Isoforms[a]

Pgp isoform	fraction labeled[c]
wild type	1.00 ± 0.06
Cys-less	0.08 ± 0.05
E393C	n/d[b]
S452C	n/d
I500C	0.29 ± 0.08
N508C	0.33 ± 0.02
K578C	0.03 ± 0.05

[a] The various purified Pgp (250 ng) isoforms were incubated with 1 μM [^{3}H]NEM for 1 h at 20 °C and then subjected to SDS−PAGE (8%) and autoradiography to determine the relative accessibilities of the introduced cysteine residues to covalent modification. Densitometric analyses were performed on autoradiograms and the labeling density observed for wild-type protein assigned a value of 1.0. The extent of labeling to each mutant Pgp was then compared to this value. [b] n/d indicates that it was not possible to accurately assign a densitometric value (see text). [c] The fractions labeled are shown as mean±sem from at least three independent protein preparations.

S452C mutant proteins were labeled with [^{3}H]-NEM; however, the presence of contaminating bands at around 140 kDa precluded accurate quantitation. As mentioned above, purification yields for these two mutants were 10−20-fold lower. Consequently, the effects of derivitization of any contaminating proteins of similar molecular weight by NEM will interfere with analysis due to insufficient electrophoretic separation of minor contaminants from Pgp mutant. Western immunoblotting analysis determined that these proteins were

Table 5: The Effects of NEM on the Extent and Potency of Drugs to Alter the ATPase Activity of N508C Pgp[a]

	nicardipine		vinblastine		paclitaxel	
	EC_{50} (μM)	stimulation	EC_{50} (μM)	stimulation	EC_{50} (μM)	stimulation
−NEM	5.3 ± 0.3	3.3 ± 0.1	8.3 ± 1.2	1.6 ± 0.1	5.1 ± 2.1	2.3 ± 0.1
+NEM	6.4 ± 0.8	3.0 ± 0.2	6.9 ± 1.7	1.5 ± 0.1	5.3 ± 2.5	2.2 ± 0.2

[a] ATP hydrolysis was measured for the N508C Pgp mutant protein (250 ng) in the presence or absence of 100 μM NEM at a range of drug concentrations (3 nM to 100 μM). The potency (EC_{50}) of each drug to stimulate ATPase activity was determined by curve fitting with the general dose−response relationship using nonlinear regression. The degree of stimulation was obtained from the ratio of the maximal ATPase activity in the presence of drug to that in its absence. EC_{50} values were determined from three independent protein preparations and are shown as mean ± SEM.

unrelated to Pgp, although they contained cysteine residues as evidenced by their efficient derivitization (data not shown). [^{3}H]-NEM was able to efficiently label mutants I500C and N508C to approximately 30% of that observed for the wild type Pgp (Table 4). Thus, the introduced cysteine residues in four of the mutants were accessible to derivitization by the NEM; however, only labeling at residue 508 altered the ATPase activity of the protein.

Derivitization with NEM is an irreversible process and therefore it is not possible to produce an equilibrium-binding constant to determine the affinity of interaction. Figure 3b shows a representative autoradiograph of the time dependent increase in [^{3}H]-NEM labeling of N508C Pgp. The data from four independent protein preparations are summarized in Figure 3c. The observed rate constant of 0.0145 ± 0.0010 min^{-1} is equivalent to the association rate constant since there is no dissociation and translates into a half-time for labeling of 49 ± 4 min. This value is comparable to the rate of derivitization of the cysteine residue within the exposed Walker A motif in soluble NBDs (*40*).

The Ability of NEM to Perturb Drug Interaction with N508C−Pgp. The data in Figure 2 demonstrated that treatment of mutant N508C with NEM produced a reduction in nicardipine stimulated ATPase activity. Is derivitization of residue 508 preventing communication between drug binding sites in the TMDs and the NBDs? To address this question the N508C protein was derivitized with 100 μM NEM and the ability of nicardipine, vinblastine, and paclitaxel to stimulate ATP hydrolysis measured. The degree of stimulation and the potency of each drug to produce the effect on underivitised and NEM-derivitized protein are shown in Table 5. Neither the extent nor the potency of drug effect on ATPase activity was affected by derivitization, suggesting that the allosteric interaction between TMD and NBD is unaffected. This was corroborated by the unaltered extent of N508C labeling by [^{3}H]-NEM (1 μM) in the presence of a fixed 30 μM concentration of nicardipine, vinblastine or paclitaxel (data not shown). These results may indicate that the inhibition of ATP hydrolysis by NEM in N508C Pgp occurs during the catalytic cycle itself rather than perturbation of allosteric influences produced by drug binding.

The Mechanism of Pgp Inhibition by Covalent Labeling of Residue 508C. To determine the molecular mechanism of the NEM induced inhibition of ATP hydrolysis through residue 508, a closer inspection of the catalytic cycle was undertaken. The data in Figure 4 demonstrate the effect of derivitization with 100 μM NEM on both the basal and vinblastine stimulated ATPase activity of Pgp. In the absence of NEM, the basal ATPase activity was stimulated 2.2-fold by the transported substrate vinblastine from 0.34 ± 0.01 μmol min^{-1} mg^{-1} ($K_{m(ATP)}$ = 0.63 ± 0.04 mM) to 0.74 ± 0.05 μmol min^{-1} mg^{-1} ($K_{m(ATP)}$ = 0.38 ± 0.01 mM). Following derivitization with NEM, the ATPase activity was also stimulated to a similar extent (2.2-fold) by vinblastine; however, the maximal activity was significantly lower at 0.34 ± 0.01 μmol min^{-1} mg^{-1} ($K_{m(ATP)}$ = 0.56 ± 0.06 mM). This decrease is primarily due to the suppression of basal ATPase activity, which at 0.15 ± 0.02 μmol min^{-1} mg^{-1} ($K_{m(ATP)}$ = 0.35 ± 0.02 mM) was only 45% of the level observed in untreated protein. This suggests that derivitization of residue 508 interferes with a fundamental step in the catalytic cycle, and therefore subsequent investigations focused on the individual stages.

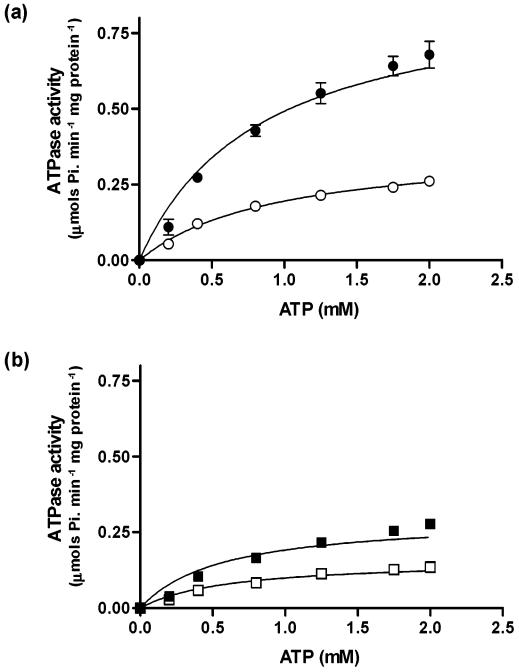

FIGURE 4: The effect of sulfydryl modification on vinblastine stimulated and basal ATPase activity of mutant N508C. The basal and drug stimulated ATPase activities were determined for N508C Pgp (250 ng) as described in the experimental procedures at different ATP concentrations (0−2 mM). (a) ATPase activity of N508C Pgp in the presence (●) or absence (○) of 30 μM vinblastine. (b) ATPase activity of N508C Pgp that had been preincubated with 100 μM NEM for 30 min at 20 °C. Catalytic activities were determined in the presence (■) or absence (□) of 30 μM vinblastine. All values represent the mean ± SEM of at least three independent protein preparations.

The initial event in the catalytic cycle is binding of nucleotide and the ability of NEM treatment to affect this parameter in wild type and N508C Pgp is shown in Figure 5. The two proteins were labeled with 3 μM [α-^{32}P]-azidoATP, the maximal achievable concentration of this

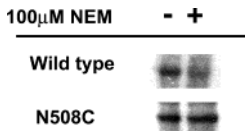

FIGURE 5: The effects of NEM on the photoaffinity labeling of Pgp by [^{32}P]-azido-ATP. Purified wild type and N508C Pgp isoforms were incubated with 3 μM Mg·[^{32}P]-azido-ATP for 20 min at 20 °C and then subjected to UV-light for 5 min at 4 °C. The extent of labeling for each isoform was compared with that following preincubation of the protein for 60 min with 100 μM NEM. The amount of cross-linking was determined by SDS−PAGE with autoradiography.

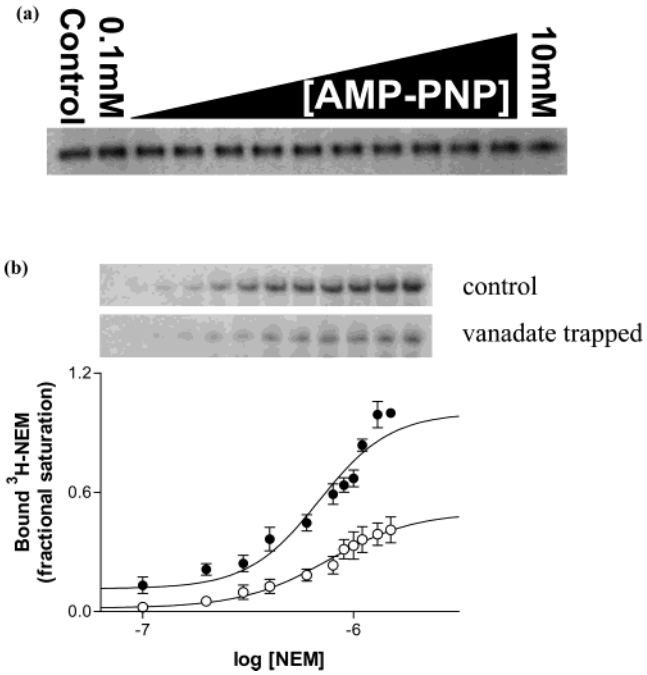

FIGURE 6: The efficiency of N508C labeling by [^{3}H]-NEM during different stages of the catalytic cycle. (a) N508C (250 ng) was labeled with [^{3}H]-NEM (1 μM) in the presence of increasing concentrations of AMP−PNP and the inset shows a representative autoradiogram. (b) N508C−Pgp was trapped with 2 mM Mg·ATP and 200 μM vanadate for 20 min at 37 °C. Control (●) and trapped (○) protein was then labeled with varying concentrations of [^{3}H]-NEM and the autoradiograms were analyzed to determine the extent of labeling at each concentration of [^{3}H]-NEM.

commercially obtained nucleotide. Labeling was performed at low temperature to prevent hydrolysis of bound nucleotide. As demonstrated in Figure 5, both the wild type and N508C Pgp isoforms were labeled with the ATP analogue. However, prior treatment of the wild-type Pgp with NEM caused a substantial reduction in the extent of labeling (consistent with the presence of a cysteine in the Walker A motif). In contrast, no effect was observed for the NEM derivitised N508C mutant isoform which displayed similar intensity of photoaffinity labeling with [α-^{32}P]-azidoATP. Therefore, the inhibition of ATP hydrolysis caused by covalent attachment of NEM to the N508C isoform was not due to impaired binding of nucleotide.

If the NEM derivitization of N508C has an inhibitory effect on ATP hydrolysis, one might expect that trapping of the N508C isoform with ADP and vanadate might exert a negative effect on the ability of NEM to label the protein. This was tested by prior trapping of the protein in the Pgp·ADP·Vi (posthydrolytic) state before labelling with [^{3}H]-NEM over a large concentration range (Figure 6b). At a concentration of 1 μM [^{3}H]-NEM the extent of labeling after a 1-h incubation was reduced by 41 ± 7% following vanadate trapping. In contrast, the non-hydrolyzable nucleotide analogue AMP−PNP up to 10 mM did not alter labeling of the nucleotide-binding domain in N508C−Pgp by 1 μM [^{3}H]-NEM (Figure 6a). This result suggests that only following hydrolysis of nucleotide does the NBD assume a conformation in which the 508C residue displays a significantly reduced accessibility to covalent labeling with [^{3}H]-NEM.

DISCUSSION

The use of site-directed mutagenesis has provided significant information on the domain organization of Pgp and the present manuscript has utilized this approach to tackle the issue of interdomain communication routes. A molecular model of the N-terminal NBD, based on the available high-resolution crystal structure of HisP, was generated to focus the mutagenesis on surface exposed residues. The interaction between the two NBDs during basal ATP hydrolysis was found to involve a conformational change that is sensitive to perturbation of the residue at position 508. The conformational change was not affected by mutation of the endogenous residue to cysteine. However, when the introduced cysteine was covalently labeled by NEM the conformational change occurred at a significantly reduced rate and the effect manifest at the post-nucleotide binding stage of the catalytic cycle.

A number of investigations, which have used site-directed mutations within the Walker A and B motifs and the signature sequence, have identified residues essential for hydrolysis of the bound nucleotide (*41*−*45*). In addition, a substantial body of information has revealed a high degree of cooperativity and communication between the two NBDs and along the NBD−TMD axis (*5*, *46*−*48*). However, our understanding of the molecular identity of residues critical to such communication routes is scant. It was therefore hypothesized that mutations should be restricted to areas of the NBDs that are not intrinsically or directly crucial to nucleotide binding and hydrolysis. Consequently, such mutations would permit nucleotide interaction with the NBD, but allow investigation of secondary effects such as the communication routes. Moreover, the use of fewer, and more highly directed, mutations would render detailed mechanistic investigations feasible. To achieve this, a model of the N-terminal NBD was devised and residues at surface exposed regions identified.

None of the residues in the expressed proteins significantly impaired function as determined by measurement of ATPase activity. In addition, the degree and potency of drugs to affect this activity were not perturbed, indicating fully preserved NBD-TMD communication. Given the surface exposed locations of the chosen residues, efficient labeling with the thiol reactive compound NEM would be expected. None of the proteins were labeled to a similar degree as the wild type protein, a finding that was consistent with the presence of multiple cysteine residues (seven in all) in the latter, two of which have previously been derivitised using thiol reactive compounds, with the consequence of such labeling resulting in full inhibition of ATP hydrolysis (*44*, *45*). Similarly, full inhibition of the ATPase activity of purified, reconstituted wild-type Pgp was observed in the present study using NEM.

The K578C mutant isoform did not display inhibition of ATPase activity by NEM, and this was attributed to the lack of detectable labeling by this maleimide-containing compound. In contrast, the E393C, S452C, and I500C isoforms were labeled by NEM, yet this did not perturb the basal or drug stimulated ATPase activity. These mutant isoforms do not provide a useful tool with which to investigate the conformational changes occurring in the catalytic cycle of Pgp. However, the ATPase activity of the N508C mutant isoform was inhibited following covalent attachment of the maleimide-containing probe. The ATP hydrolytic cycle is a complex and multistep process (*19*). Therefore, a more detailed examination of individual stages of the catalytic cycle was undertaken to provide a molecular mechanism for the nature of NEM induced inhibition of the N508C isoform.

The principle questions to be addressed were whether the inhibition was directed at basal or drug stimulated activity and did it prevent ATP binding, hydrolysis or ADP (+ Pi) dissociation from the protein? On first inspection, derivitization of the N508C protein with NEM caused a large decrease in the maximal velocity of drug stimulated ATP hydrolysis. However, regardless of the drug used, the degree to which basal ATPase activity was stimulated and the potency of several chemically distinct drugs to alter the activity remained unchanged. This indicates that the formation of a covalent attachment with NEM at residue 508 did not perturb the route of communication between drug binding sites in the TMDs with the catalytic region of the NBDs. The basal ATPase activity of N508 Pgp was however inhibited by NEM. Basal activity requires two functional NBDs to maintain overall hydrolysis (*44*) and a high degree of cooperativity between the two domains during a catalytic cycle (*18*). This suggests that conformational changes during ATP hydrolysis are prevented by covalent attachment of NEM to residue 508C.

The derivitization by NEM may alter basal ATP hydrolysis by preventing the binding of nucleotide to the NBD or through inhibition of the chemical hydrolysis of the γ-phosphate group in ATP. The binding of nucleotide appears unaffected by derivitization since the affinity constant for hydrolysis ($K_m = (k_1 + k_2)/k_{-1}$) was not altered and this parameter is sensitive to both association (k_1) and dissociation rate (k_{-1}) constants for nucleotide binding. In addition, albeit at low concentrations of nucleotide, the extent of [α^{32}P]-8-azido-ATP labeling of N508C Pgp was unaffected by prior interaction with NEM. Clearly, the inhibitory effect of NEM is manifest at a subsequent stage of the catalytic cycle. The demonstration that the non-hydrolyzable ATP analogue AMP−PNP did not impair labeling of N508C suggests that this residue does not become buried upon ATP binding, despite the considerable conformational changes the NBD undergoes (*49*−*51*).

The vanadate trapping technique (*17*) provides a useful tool to determine whether the inhibitory effect of NEM on the N508C Pgp isoform occurs immediately posthydrolysis of the γ-phosphate group. The extent to which N508C Pgp was covalently labeled by [^{3}H]-NEM was significantly impaired following vanadate trapping of the protein. This suggests that the conformational changes occurring after cleavage of the γ-phosphate cause residue 508 to adopt a configuration that is inaccessible to derivitization with NEM. By inference, the prior covalent attachment of NEM to N508C would be expected to prevent or retard the previously reported conformational changes immediately following ATP hydrolysis (*12*, *13*, *52*). At present, it is only possible to assign the changes as "posthydrolysis" and not attribute them to a specific intermediate stage such as following the chemical hydrolysis step, Pi dissociation or ADP release. Quantitative analysis of such events is technically not feasible at present. It is possible that perturbation of conformational changes following nucleotide hydrolysis would lower the rate of ATPase activity by retarding communication between the two NBDs during catalysis. Our results appear to confirm this and one possible explanation is that conformational changes are required for cooperativity between NBDs.

Recently, the structures of several NBD dimers in which ATP coordination involves residues from both NBDs (*26*, *33*) have been described. Inspection of the arrangement in BtuCD and MJ0796 demonstrates that the equivalent residue to Pgp-N508 is in the α-helical subdomain and exposed on the accessible surface of the NBD dimer of both structures. Furthermore, short (*53*) and long (Campbell, J. C., Kerr, I. D., and Sansom, M. S. P., unpublished observations) timescale molecular dynamics simulations of ABC transporter NBDs provide evidence that the α-helical subdomain displays conformational changes in response to nucleotide binding. This molecular modeling data are consistent with our experimental evidence demonstrating that residue 508 is involved in conformational changes required to maintain ATP hydrolysis.

ACKNOWLEDGMENT

We thank the indomitable Dr. Andrew "Reg" Rose for inspiring the work leading to this manuscript and the group headed by Prof. Linda King at Oxford Brookes University for their assistance with the baculovirus expression system. The contribution of XR9576 by Xenova Ltd was also greatly appreciated.

REFERENCES

1. Bates, S. F., Chen, C., Robey, R., Kang, M., Figg, W. D., and Fojo, T. (2002) *Novartis Found. Symp. 243*, 83−96.
2. Gottesman, M. M., Fojo, T., and Bates, S. E. (2002) *Nat. Rev. Cancer 2*, 48−58.
3. Higgins, C. F. (1992) *Annu. Rev. Cell. Biol. 8*, 67−113.
4. Bruggemann, E. P., Currier, S. J., Gottesman, M. M., and Pastan, I. (1992) *J. Biol. Chem. 267*, 21020−6.
5. al-Shawi, M. K., and Senior, A. E. (1993) *J. Biol. Chem. 268*, 4197−206.
6. Loo, T. W., and Clarke, D. M. (2001) *J. Biol. Chem. 276*, 14972−9.
7. Loo, T. W., and Clarke, D. M. (1999) *J. Biol. Chem. 274*, 35388−35392.
8. Urbatsch, I. L., Sankaran, B., Bhagat, S., and Senior, A. E. (1995) *J Biol. Chem. 270*, 26956−26961.
9. Martin, C., Berridge, G., Higgins, C. F., Mistry, P., Charlton, P., and Callaghan, R. (2000) *Mol. Pharmacol. 58*, 624−632.
10. Shapiro, A. B., and Ling, V. (1997) *Eur. J. Biochem. 250*, 130−7.
11. Ambudkar, S. V., Dey, S., Hrycyna, C. A., Ramachandra, M., Pastan, I., and Gottesman, M. M. (1999) *Annu. Rev. Pharmacol. Toxicol. 39*, 361−398.
12. Martin, C., Higgins, C. F., and Callaghan, R. (2001) *Biochemistry 40*, 15733−42.
13. Rosenberg, M. F., Velarde, G., Ford, R. C., Martin, C., Berridge, G., Kerr, I. D., Callaghan, R., Schmidlin, A., Wooding, C., Linton, K. J., and Higgins, C. F. (2001) *EMBO J. 20*, 5615−25.
14. Pascaud, C., Garrigos, M., and Orlowski, S. (1998) *Biochem. J. 333*, 351−358.

15. Loo, T. W., and Clarke, D. M. (1994) *J. Biol. Chem. 269*, 7750−5.
16. Loo, T. W., and Clarke, D. M. (1995) *J. Biol. Chem. 270*, 22957−22961.
17. Urbatsch, I. L., Sankaran, B., Weber, J., and Senior, A. E. (1995) *J. Biol. Chem. 270*, 19383−90.
18. Urbatsch, I. L., Sankaran, B., Bhagat, S., and Senior, A. E. (1995) *J. Biol. Chem. 270*, 26956−61.
19. Senior, A. E., Al-Shawi, M. K., and Urbatsch, I. L. (1995) *FEBS Lett. 377*, 285−289.
20. Julien, M., and Gros, P. (2000) *Biochem. 39*, 4559−68.
21. Druley, T. E., Stein, W. D., and Roninson, I. B. (2001) *Biochemistry 40*, 4312−22.
22. Sonveaux, N., Vigano, C., Shapiro, A. B., Ling, V., and Ruysschaert, J. M. (1999) *J. Biol. Chem. 274*, 17649−54.
23. Liu, R., Siemiarczuk, A., and Sharom, F. J. (2000) *Biochemistry 39*, 14927−38.
24. Rosenberg, M. F., Kamis, A. B., Callaghan, R., Higgins, C. F., and Ford, R. C. (2003) *J. Biol. Chem. 278*, 8294−9.
25. Hung, L.-W., Wang, I. X., Nikaido, K., Ardeshir, F., Garcia, G., and Ames, G. F.-L. (1998) *Nature 396*, 703−707.
26. Hopfner, K. P., Karcher, A., Shin, D. S., Craig, L., Arthur, L. M., Carney, J. P., and Tainer, J. A. (2000) *Cell 101*, 789−800.
27. Diedrichs, K., Diez, J., Greller, G., Muller, C., Breed, J., Schnell, C., Vonrhein, C., Boos, W., and Welte, W. (2000) *EMBO J. 19*, 5951−5961.
28. Kerr, I. D. (2002) *Biochim. Biophys. Acta 1561*, 47−64.
29. Locher, K. P., Lee, A. T., and Rees, D. C. (2002) *Science 296*, 1091−8.
30. Chang, G., and Roth, C. B. (2001) *Science 293*, 1793−800.
31. Sali, A., and Blundell, T. L. (1993) *J. Mol. Biol. 234*, 779−815.
32. Smith, P. C., Karpowich, N., Millen, L., Moody, J. E., Rosen, J., Thomas, P. J., and Hunt, J. F. (2002) *Mol. Cell 10*, 139−49.
33. Karpowich, N., Martsinkevich, O., Millen, L., Yuan, Y. R., Dai, P. L., MacVey, K., Thomas, P. J., and Hunt, J. F. (2001) *Structure (Camb.) 9*, 571−86.
34. Blott, E. J., Higgins, C. F., and Linton, K. J. (1999) *EMBO J. 18*, 6800−6808.
35. Taylor, A. M., Storm, J., Soceneantu, L., Linton, K. J., Gabriel, M., Martin, C., Woodhouse, J., Blott, E., Higgins, C. F., and Callaghan, R. (2001) *Br. J. Pharmacol. 134*, 1609−18.
36. Page, M. J., and Rodgers, B. C. (1995) *Methods Mol. Biol. 39*, 107−27.
37. Chifflet, S., Chiesa, U. T. R., and Tolosa, S. (1988) *Anal. Biochem. 168*, 1−4.
38. Morris, A. L., MacArthur, M. W., Hutchinson, E. G., and Thornton, J. M. (1992) *Proteins 12*, 345−64.
39. Gaudet, R., and Wiley, D. C. (2001) *EMBO J. 20*, 4964−72.
40. Berridge, G., Walker, J., Callaghan, R., and Kerr, I. D. (2003) *Eur. J. Biochem. 270*, 1483−1492.
41. Bakos, E., Klein, I., Welker, E., Szabo, K., Muller, M., Sarkadi, B., and Varadi, A. (1997) *Biochem. J. 323*, 777−83.
42. Beaudet, L., Urbatsch, I. L., and Gros, P. (1998) *Biochemistry 37*, 9073−9082.
43. Hrycyna, C. A., Ramachandra, M., Germann, U. A., Cheng, P. W., Pastan, I., and Gottesman, M. M. (1999) *Biochemistry 38*, 13887−13899.
44. Loo, T. W., and Clarke, D. M. (1995) *J. Biol. Chem. 270*, 22957−61.
45. Urbatsch, I. L., Gimi, K., Wilke-Mounts, S., Lerner-Marmarosh, N., Rousseau, M. E., Gros, P., and Senior, A. E. (2001) *J. Biol. Chem. 276*, 26980−7.
46. Sarkadi, B., Price, E. M., Boucher, R. C., Germann, U. A., and Scarborough, G. A. (1992) *J. Biol. Chem. 267*, 4854−8.
47. al-Shawi, M. K., Urbatsch, I. L., and Senior, A. E. (1994) *J. Biol. Chem. 269*, 8986−92.
48. Qu, Q., and Sharom, F. J. (2001) *Biochemistry 40*, 1413−22.
49. Schneider, E., Wilken, S., and Schmid, R. (1994) *J. Biol. Chem. 269*, 20456−61.
50. Mourez, M., Hofnung, M., and Dassa, E. (1997) *EMBO J. 16*, 3066−3077.
51. Kreimer, D. I., Chai, K. P., and Ames, G. F.-L. (2000) *Biochemistry 39*, 14183−14195.
52. Sonveaux, N., Vigano, C., Shapiro, A. B., Ling, V., and Ruysschaert, J. M. (1999) *J. Biol. Chem. 274*, 17649−17654.
53. Jones, P. M., and George, A. M. (2002) *Proc. Natl. Acad. Sci. U.S.A. 99*, 12639−44.

BI0341049